ПИ
I-65

Inorganic Chemistry

including bioinorganic chemistry

January 20, 2014
Volume 53, Number 2
pubs.acs.org/IC

Probing Orientational Disorder in Oxides

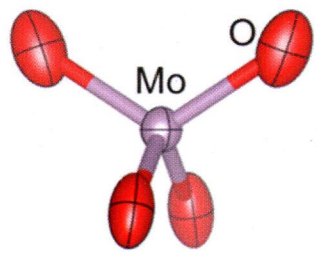

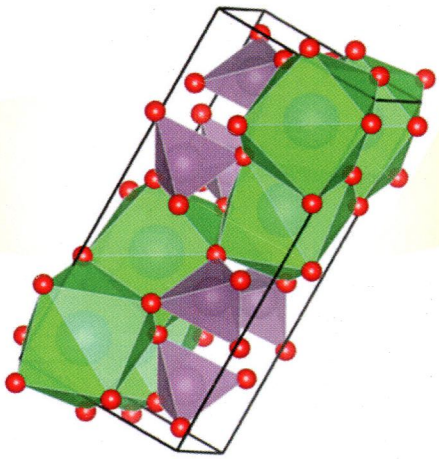

$(Ca, Sr, Ba)MoO_4$

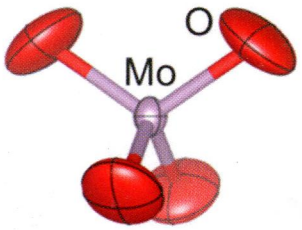

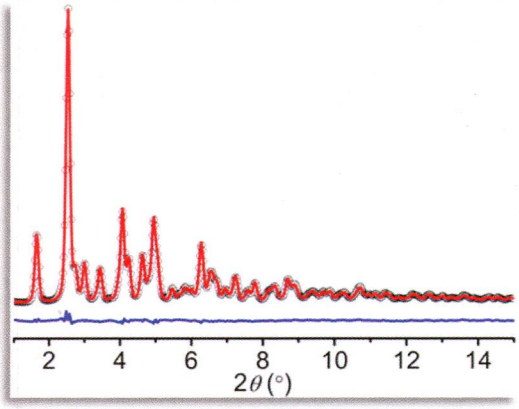

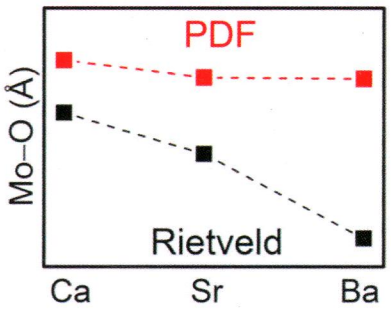

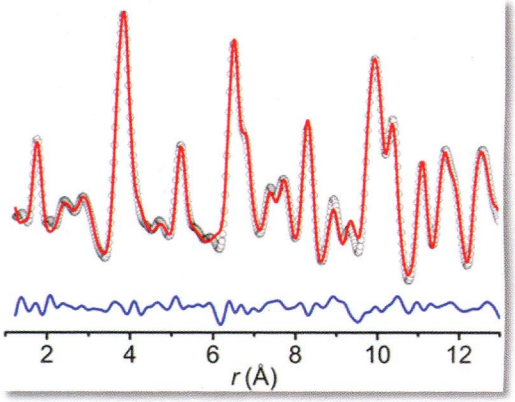

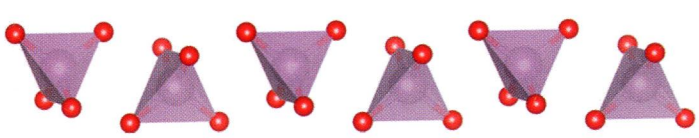

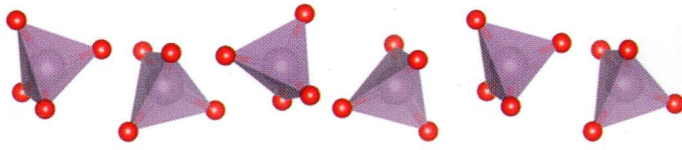

ACS Publications
MOST TRUSTED. MOST CITED. MOST READ.

www.acs.org

Inorganic Chemistry

JANUARY 20, 2014
VOLUME 53 ISSUE 2

INOCAJ 53(2) 661−1256 (2014)
ISSN 0020-1669
Registered in the U.S. Patent and Trademark Office
© 2014 by the American Chemical Society

ON THE COVER: A dual-space approach combining Rietveld and pair distribution function analysis of X-ray diffraction data was used to probe orientational disorder in $AMoO_4$ (A = Ca, Sr, Ba) scheelite oxide nanocrystals. See F. A. Rabuffetti, S. P. Culver, L. Suescun, and R. L. Brutchey, p 1056.

Communications

661 Ⓢ dx.doi.org/10.1021/ic402063f

π-Back-Bonding Interaction Depending on the Bridging Chain Lengths of Chelated N-Heterocyclic Carbene Platinum Units in Heterometallic Trinuclear Complexes Affecting Their Electrochemical Property
Yuri Maeda, Hideki Hashimoto, Isamu Kinoshita, and Takanori Nishioka*

Variation of the dihedral angles caused by different bridging chain lengths of chelating NHC ligands in heterometallic trinuclear complexes containing platinum bis-N-heterocyclic carbene units affected the redox potentials of trinuclear complexes.

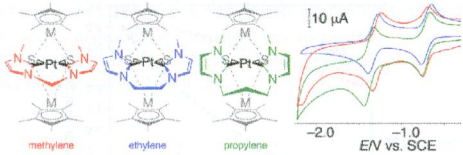

664 Ⓢ dx.doi.org/10.1021/ic402108w

Catalytic Reduction of Hydrazine to Ammonia by a Mononuclear Iron(II) Complex on a Tris(thiolato)phosphine Platform
Ya-Ho Chang, Pooi-Mun Chan, Yi-Fang Tsai, Gene-Hsiang Lee, and Hua-Fen Hsu*

We obtained an iron(II) complex supported by a tris(thiolato)phosphine ligand that shows the catalytic reactivity in the reduction of hydrazine, an intermediate and a substrate of nitrogenase. The substrate- and product-bound adducts were also synthesized independently and structurally characterized. The work provides the feasibility that the late stage of biological nitrogen fixation can be conducted at a single iron site with a sulfur-rich ligation environment.

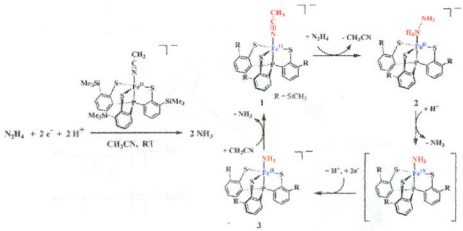

667 S dx.doi.org/10.1021/ic4021178

A Novel Heterometallic μ_9-Boride Cluster: Synthesis and Structural Characterization of $[(\eta^5\text{-}C_5Me_5Rh)_2\{Co_6(CO)_{12}\}(\mu\text{-}H)(BH)B]$

Dipak Kumar Roy, Subrat Kumar Barik, Bijan Mondal, Babu Varghese, and Sundargopal Ghosh*

The reaction of *nido*-$[(Cp^*Rh)_2B_2H_6]$ ($Cp^* = \eta^5\text{-}C_5Me_5$) with $[Co_2(CO)_8]$ yielded the first heterometallic M_8-boride cluster $[(Cp^*Rh)_2\{Co_6(CO)_{12}\}(\mu\text{-}H)(BH)B]$.

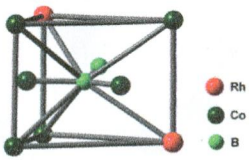

670 S dx.doi.org/10.1021/ic402126e

An Unusual Metallic Oxygen Cluster Consisting of a $\{AlMo_{12}O_{40}(MoO_2)\}$

Zhan-Gang Han,* Xiao-Qing Chang, Jin-Shuang Yan, Kai-Ning Gong, Chuan Zhao, and Xue-Liang Zhai*

A novel aluminum-containing, bimolybdenum-capped Keggin-type polyoxomolybate cluster of the $\{AlMo_{12}O_{40}(MoO_2)_2\}$ anion has been experimentally determined.

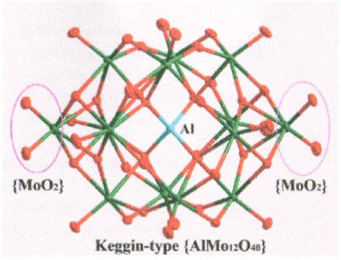

673 S dx.doi.org/10.1021/ic402262z

$LiPbSb_3S_6$: A Semiconducting Sulfosalt with Very Low Thermal Conductivity

Eva C. Agha, Christos D. Malliakas, Jino Im, Hosub Jin, Li-Dong Zhao, Arthur J. Freeman, and Mercouri G. Kanatzidis*

The semiconducting sulfosalt $LiPbSb_3S_6$ is composed of layers of PbS archetype Sb/Li–S separated by trigonal-prismatic-coordinated Pb/Li. This compound has one of the lowest thermal conductivities seen in a crystalline material and a high resistivity and exhibits a nearly direct band gap of 1.6 eV.

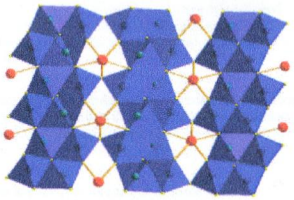

676 dx.doi.org/10.1021/ic402256v

Huge Magnetic Anisotropy in a Trigonal-Pyramidal Nickel(II) Complex

Silvia Gómez-Coca,* Eduard Cremades, Núria Aliaga-Alcalde, and Eliseo Ruiz*

Experimental and theoretical studies of a mononuclear nickel(II) complex with the largest magnetic anisotropy ever reported. Zero-field-splitting D parameter, extracted from the fits of the magnetization and susceptibility measurements, shows a large value of -200 cm^{-1}, in agreement with the theoretical value of -244 cm^{-1} obtained with the CASPT2–RASSI method.

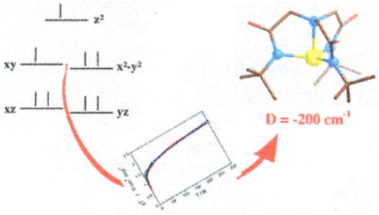

679 dx.doi.org/10.1021/ic402430n

Drastic Enhancement of the CO_2 Adsorption Properties in Sulfone-Functionalized Zr- and Hf-UiO-67 MOFs with Hierarchical Mesopores

Pantelis Xydias, Ioannis Spanopoulos, Emmanuel Klontzas, George E. Froudakis, and Pantelis N. Trikalitis*

The sulfone-functionalized Zr- and Hf-UiO-67 materials with hierarchical mesopores show a drastic enhancement of CO_2 uptake and CO_2/CH_4 selectivity compared to the parent UiO-67 solid.

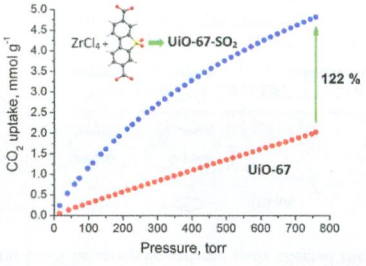

682 dx.doi.org/10.1021/ic402513d

Magnetic Structure and Properties of the Rechargeable Battery Insertion Compound Na_2FePO_4F

Maxim Avdeev,* Chris D. Ling, Thiam Teck Tan, Sean Li, Gosuke Oyama, Atsuo Yamada, and Prabeer Barpanda

Na_2FePO_4F was studied experimentally using magnetometry and neutron powder diffraction. Below 3.4 K, the material magnetically orders to a noncollinear structure of ferromagnetically ordered face- and vertex-sharing zigzag chains of $[FeO_4F_2]$, coupled antiferromagnetically by super-super-exchange via phosphate groups.

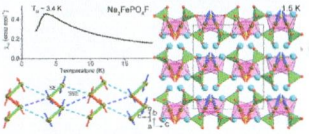

685 S dx.doi.org/10.1021/ic402598p

Conversion from a Heterochiral [2 + 2] Coaxially Nested Double-Helical Column to a Cationic Spiral Staircase Stimulated by an Ionic Liquid Anion

Jianhua Qin, Yanyuan Jia, Huijun Li, Bei Zhao, Dongqing Wu, Shuangquan Zang,* Hongwei Hou,* and Yaoting Fan

The conversion from a [2 + 2] nested double-helical column, $\{[Mn_2(ptptp)(suc)(H_2O)_2]\cdot 1.5H_2O\}_n$ (**1**), to a cationic spiral staircase, $\{[Mn_2(ptptp)(suc)_{0.5}(H_2O)_3]\cdot Br\cdot 0.5H_2O\}_n$ (**2**), has been achieved through ionic-liquid-anion stimulation under solvothermal conditions, and variable-temperature magnetic susceptibility reveals that the conversion does not change the antiferromagnetic interactions.

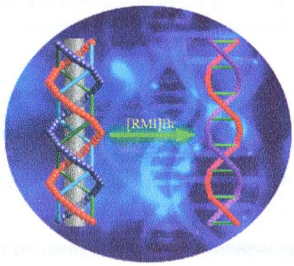

688 S dx.doi.org/10.1021/ic402686s

Self-Assembly of an Imidazolate-Bridged Fe^{III}/Cu^{II} Heterometallic Cage

Florian Reichel, Jack K. Clegg,* Karsten Gloe, Kerstin Gloe, Jan J. Weigand, Jason K. Reynolds, Chun-Guang Li, Janice R. Aldrich-Wright, Cameron J. Kepert, Leonard F. Lindoy, Hong-Chang Yao, and Feng Li*

An imidazolate-bridged Fe^{III}/Cu^{II} heterometallic nanocage has been synthesized by coordination-driven face-directed self-assembly using a suitable metalloligand.

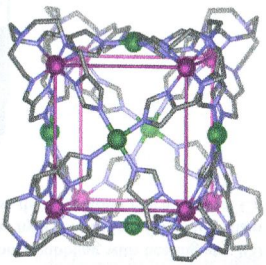

691 S dx.doi.org/10.1021/ic402692p

Growing Crystalline Zinc-1,3,5-benzenetricarboxylate Metal–Organic Frameworks in Different Surfactants

Junkuo Gao, Kaiqi Ye, Ling Yang, Wei-Wei Xiong, Ling Ye, Yue Wang, and Qichun Zhang*

Six new zinc-1,3,5-benzenetricarboxylate-based metal–organic frameworks (MOFs) were successfully synthesized by a surfactant–thermal method. Three different surfactants with neutral, acidic, and cationic characteristics, respectively, were used as the reaction media.

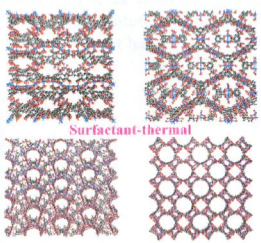

694 S dx.doi.org/10.1021/ic402806x

Uranium(IV) Imidazolin-2-iminato Complexes: A New Class of Actinide Complexes

Isabell S. R. Karmel, Mark Botoshansky, Matthias Tamm,* and Moris S. Eisen*

A family of uranium(IV) imidazolin-2-iminato complexes was synthesized by the reaction between $U(NMeEt)_4$ and the neutral imidazolin-2-iminato ligands Im^RNH. The complexes $[U(NIm^{tBu})_4]$ (**1**), $[U(NIm^{Mes})_3(NMeEt)]$ (**2**), and $[U(NIm^{Dipp})_2(NMeEt)_2]$ (**3**) were obtained depending on the steric demand of the substituent R, displaying short U−N bonds and large U−N−C bond angles. Complex **3** showed extraordinarily high activity toward the polymerization of ε-caprolactone.

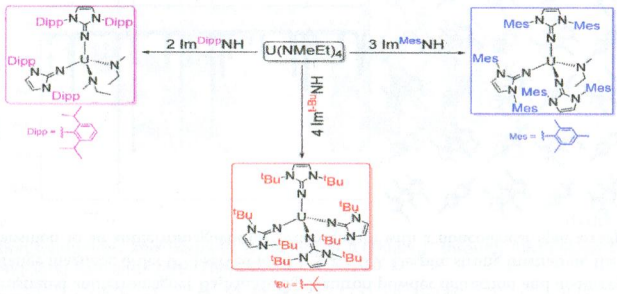

697 S dx.doi.org/10.1021/ic402885k

High Pressure Synthesis of Marcasite-Type Rhodium Pernitride

Ken Niwa,* Dmytro Dzivenko, Kentaro Suzuki, Ralf Riedel, Ivan Troyan, Mikhail Eremets, and Masashi Hasegawa

Novel noble metal nitride, RhN_2, with a marcasite-type structure was successfully synthesized in a direct chemical reaction between a rhodium metal and molecular nitrogen at 43.2 GPa using a laser-heated diamond-anvil cell.

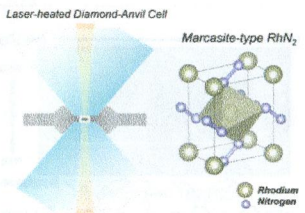

Articles

700 dx.doi.org/10.1021/ic402253y

Structural Diversity of Copper(I) Complexes Formed by Pyrrole- and Dipyrrolylmethane-Based Diphosphine Ligands with Cu–X···HN Hydrogen Bonds

Shanish Kumar, Ganesan Mani,* Debodyuti Dutta, and Sabyashachi Mishra

Two classes of pyrrole-based diphosphine ligands afforded Cu(I) complexes of the type: rhombic, tricoordinate, cubane-like, and heteroleptic. They all exhibit the substrate directing Cu–X···HN hydrogen bonds in their solid state structures, which are confirmed by NBO, AIM, and Hirshfeld analyses.

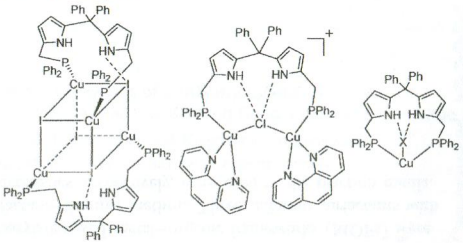

710 dx.doi.org/10.1021/ic4011604

Preparation of Copper Nitride (Cu_3N) Nanoparticles in Long-Chain Alcohols at 130–200 °C and Nitridation Mechanism

Takashi Nakamura,* Hiromichi Hayashi, Taka-aki Hanaoka, and Takeo Ebina

Copper nitride nanoparticles have been prepared in long-chain alcohol solvents with ammonia bubbling with heating at <200 °C and have been characterized. Here, we demonstrate that the reaction temperature and the hydrophobicity of the long-chain alcohols influence on the crystal structure of obtained nanoparticles. Furthermore, we discuss the nitridation mechanism of Cu ions based on measurements of GC-MS, UV-vis absorption spectra.

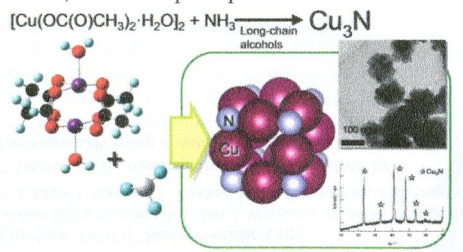

716 dx.doi.org/10.1021/ic401459a

Trinuclear and Tetranuclear Magnesium Alkoxide Clusters as Highly Active Initiators for Ring-Opening Polymerization of L-Lactide

Yuan Gao, Zhongran Dai, Jinjin Zhang, Xinxian Ma, Ning Tang, and Jincai Wu*

Four magnesium alkoxide clusters with triangular or rhombic structures were readily synthesized and fully characterized. These clusters are found to be excellent initiators for ring-opening polymerizations (ROPs) of L-lactide (L-LA) and afford polylactides desired molecular weights and narrow PDIs. Complex **2** was even able to catalyze the ROP of 4000 equiv of L-LA in 1 min with the controlled model.

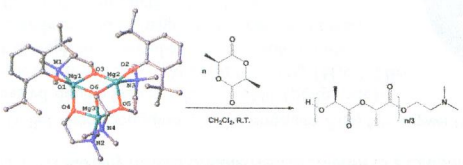

727 dx.doi.org/10.1021/ic401529u

Rhodium, Iridium, and Ruthenium Half-Sandwich Picolinamide Complexes as Anticancer Agents

Zahra Almodares, Stephanie J. Lucas, Benjamin D. Crossley, Aida M. Basri, Christopher M. Pask, Andrew J. Hebden, Roger M. Phillips, and Patrick C. McGowan*

Novel rhodium, iridium, and ruthenium half-sandwich complexes containing (*N*,*N*)-bound picolinamide ligands have been prepared for use as anticancer agents. The complexes show promising cytotoxicities, with the presence, position, and number of halides having a significant effect on the corresponding IC_{50} values.

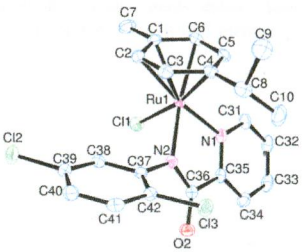

737 dx.doi.org/10.1021/ic4025052

Unichromophoric Platinum-Acetylides That Contain Pentiptycene Scaffolds: Torsion-Induced Dual Emission and Steric Shielding of Dynamic Quenching

Che-Jen Lin, Chih-Yuan Chen, Sandip Kumar Kundu, and Jye-Shane Yang*

Platinum acetylides that contain the rigid bulky pentiptycene groups near the Pt center display dual emissions with the emission color being highly sensitive to the concentration of molecular oxygen, corresponding to potential unichromophoric ratiometric oxygen probes. The role of the pentitpycene scaffolds in determining the molecular conformation and thus the photophysical and electrochemical properties is discussed with a series of related systems of varied number and position of pentiptycene groups.

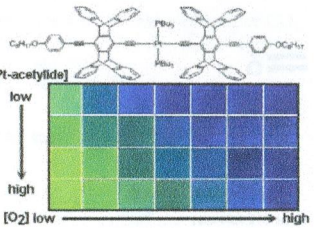

746 dx.doi.org/10.1021/ic4017799

Structural and Magnetic Study of Order–Disorder Behavior in the Double Perovskites $Ba_2Nd_{1-x}Mn_xMoO_6$

Fiona C. Coomer and Edmund J. Cussen*

The solid solution $Ba_2Nd_{1-x}Mn_xMoO_6$ was synthesized to investigate the effect of doping Jahn–Teller active Mo^{5+} into the cubic, geometrically frustrated antiferromagnet Ba_2MnMoO_6. Neutron powder diffraction and *dc*-susceptibility measurements indicate that no long-range magnetic order is observed for $0.1 \leq x < 0.9$. Despite strong frustration, the cubic $x = 0.9$ member undergoes a phase transition to an antiferromagnetically ordered state with a noncollinear spin arrangement.

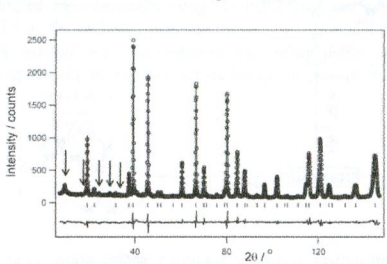

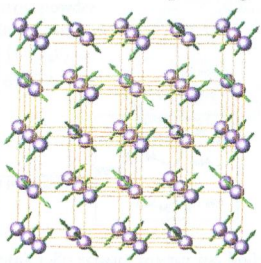

756 dx.doi.org/10.1021/ic401841n

Tuning the Luminescent Properties of Pt(II) Acetylide Complexes through Varying the Electronic Properties of N-Heterocyclic Carbene Ligands

Yuzhen Zhang, Jessica Clavadetscher, Michael Bachmann, Olivier Blacque, and Koushik Venkatesan*

A series of Pt(II) bis acetylide complexes bearing electronically different chelating NHC ligands were investigated. The varying extent of the quantum efficiencies of the deep blue emission of the different complexes is strongly suggestive of the impact of the NHC ligand on the triplet manifold.

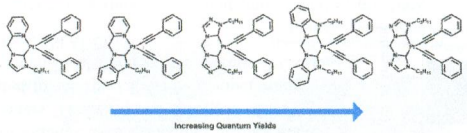

772 dx.doi.org/10.1021/ic401992y

Mercury Methylation by HgcA: Theory Supports Carbanion Transfer to Hg(II)

Jing Zhou, Demian Riccardi, Ariana Beste, Jeremy C. Smith, and Jerry M. Parks*

Density functional theory is used to explore methyl transfer reactions to Hg(II) complexes with a model of the corrinoid protein HgcA, which plays a key role in bacterial mercury methylation. Cys thiolate coordination to Co favors carbanion transfer over radical transfer to Hg(II) in the condensed phase.

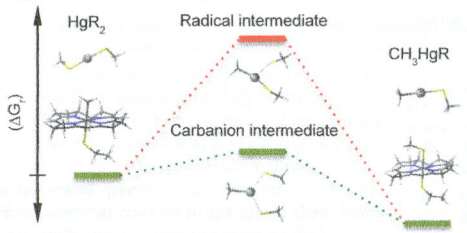

778 dx.doi.org/10.1021/ic401999r

Nature of Zr-Monosubstituted Monomeric and Dimeric Polyoxometalates in Water Solution at Different pH Conditions: Static Density Functional Theory Calculations and Dynamic Simulations

Pablo Jiménez-Lozano, Jorge J. Carbó,* Alain Chaumont,* Josep M. Poblet, Antonio Rodríguez-Fortea, and Georges Wipff

Static DFT calculations and dynamic simulations (classical and Car−Parrinello molecular dynamics) were performed to study the nature of Zr-monsubstitued monomeric and dimeric polyoxometalates in water at different pH. The Zr atom fluctuates within the oxide POM framework, providing a flexible coordination environment. At acidic conditions protonation occurs mainly at the Zr-hydroxo group favoring the formation of Zr-aqua species and dimer dissociation, whereas at basic conditions, the Zr-hydroxo species prevails promoting the Zr···Zr linkages.

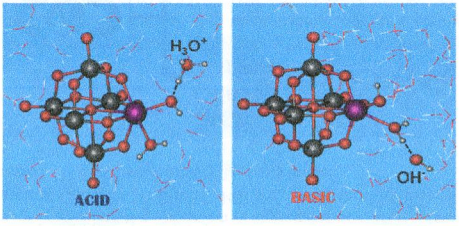

787 S dx.doi.org/10.1021/ic4020702

Structure, Phonon Properties, and Order–Disorder Transition in the Metal Formate Framework of $[NH_4][Mg(HCOO)_3]$

Mirosław Mączka,* Adam Pietraszko, Bogusław Macalik, and Krzysztof Hermanowicz

We report the synthesis and temperature-dependent studies of $[NH_4][Mg(HCOO)_3]$ formate, which belongs to chiral metal–organic frameworks of $[NH_4][M(HCOO)_3]$ (M = divalent cation), exhibiting ferroelectric and multiferroelectric properties. These studies show that $[NH_4][Mg(HCOO)_3]$ undergoes a phase transition at around 255 K from the paraelectric $P6_322$ structure to the ferroelectric $P6_3$ structure. The phase transition is due to two steps of freezing of the motion of NH_4^+ on cooling. The motional freezing becomes nearly complete below 140 K.

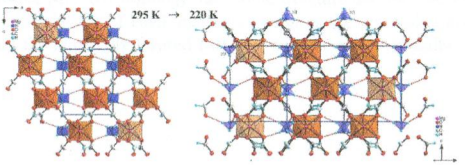

795 S dx.doi.org/10.1021/ic402111v

Tuning the Coordination Geometries and Magnetic Dynamics of $[Ln(hfac)_4]^-$ through Alkali Metal Counterions

Dai Zeng, Min Ren, Song-Song Bao, and Li-Min Zheng*

Four lanthanide compounds $[Cs\{Dy(hfac)_4\}]$ (**1**), $[Cs\{Er(hfac)_4\}]$ (**2**), $[K\{Dy(hfac)_4\}]$ (**3**), and $[K\{Er(hfac)_4\}]$ (**4**) (hfac = hexafluoroacetylacetone) are reported. All display chain structures in which the mononuclear $[Ln(hfac)_4]^-$ anions are linked by alkali metal ions. The magnetic dynamics of these complexes is strongly influenced by the cations, and field-induced slow magnetization relaxation is observed only in the potassium compounds **3** and **4** above 1.8 K.

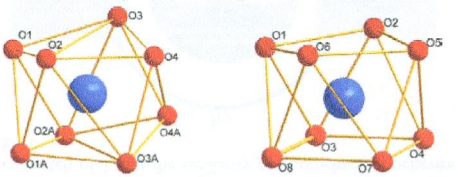

802 S dx.doi.org/10.1021/ic4020898

Preparation and Magnetic Properties of Metal-Complexes from *N*-*t*-Butyl-*N*-oxidanyl-2-amino-(nitronyl nitroxide)

Takanori Furui, Shuichi Suzuki, Masatoshi Kozaki, Daisuke Shiomi, Kazunobu Sato, Takeji Takui, Keiji Okada,*
Evgeny V. Tretyakov, Svyatoslav E. Tolstikov, Galina V. Romanenko, and Victor I. Ovcharenko*

Metal complexation reactions of *N*-*t*-butyl-*N*-oxidanyl-2-amino(nitronyl nitroxide) diradical (**1**) with $M(hfac)_2$ (M: Mn or Cu) were investigated; the Mn complex $[Mn(hfac)_2 \cdot \mathbf{1}]$ was readily prepared by mixing their components, whereas a polymer-chain complex, $[Cu_2(hfac)_2 \cdot \mathbf{3}_2 \cdot Cu(hfac)_2]_n$ (**3**: *N*-*t*-butyl-*N*-oxidanide-2-amino(iminonitroxide) radical anion), was produced through multistep redox reactions. Crystal structures of these complexes were clarified, and their magnetic properties were investigated in detail.

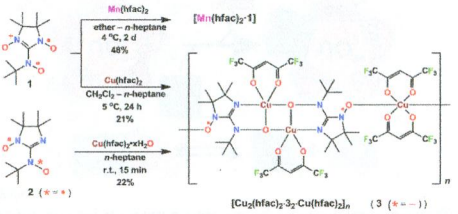

810 S dx.doi.org/10.1021/ic402099x

Design, Synthesis, and Optoelectronic Properties of Dendrimeric Pt(II) Complexes and Their Ability to Inhibit Intermolecular Interaction

Hui Li, Jing Li, Junqiao Ding, Wei Yuan, Zilong Zhang, Luyi Zou, Xingdong Wang, Hongmei Zhan,* Zhiyuan Xie, Yanxiang Cheng, and Lixiang Wang

Dendrimeric Pt(II) complexes exhibited improved emission properties including increased φ_p, enhanced EL efficiency, and slow efficiency roll-off due to effectively avoiding the formation of aggregates or excimers by incorporating bulky *t*-butyl group or adopting a homoleptic configuration. Complex [(*t*-BuCzCzPBI)Pt(dpm)] showed the best current efficiencies of 29.31 cd/A (EQE 9.04%) in solution-processed OLEDs based on Pt(II) dendrimers.

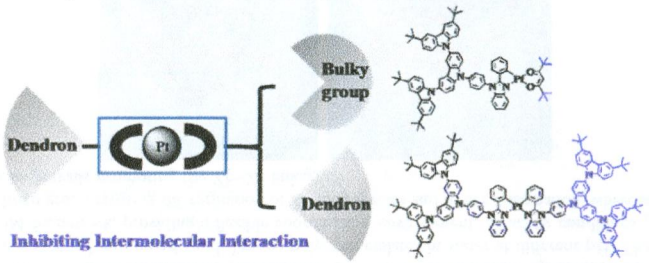

822 S dx.doi.org/10.1021/ic402127x

Synthesis and Single Crystal Structure of Sodium Octahydrotriborate, NaB_3H_8

Andrew C. Dunbar, Joseph A. Macor, and Gregory S. Girolami*

This paper describes a modified synthesis of NaB_3H_8 by the reduction of BH_3·THF with sodium dispersed on silica gel. Single crystals obtained from CH_2Cl_2 show conclusively that the space group is $Pmn2_1$, in contrast to the *Pmmn* space group previously deduced from powder diffraction data.

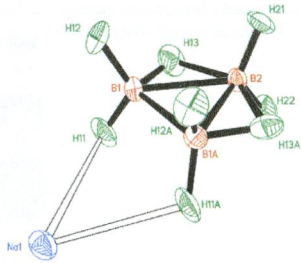

827 dx.doi.org/10.1021/ic402169w

Abnormal Reduction, $Eu^{3+} \rightarrow Eu^{2+}$, and Defect Centers in Eu^{3+}-Doped Pollucite, $CsAlSi_2O_6$, Prepared in an Oxidizing Atmosphere

Hongde Xie, Juan Lu, Ying Guan, Yanlin Huang, Donglei Wei, and Hyo Jin Seo*

Eu^{2+} ions can be obtained by heating Eu^{3+}-doped pollucite ($CsAlSi_2O_6$) in air or in a reducing atmosphere. However, the two reduction mechanisms are very different resulting in the different luminescence colors and distinct micro-structural defects around Eu^{2+} centers. The abnormal reduction of $Eu^{3+} \rightarrow Eu^{2+}$ in air atmosphere is closely related to the special charge compensation mechanism and the rigid three-dimensional framework structure of $CsAlSi_2O_6$ containing tetrahedral anion groups, $(Si,Al)O_4$.

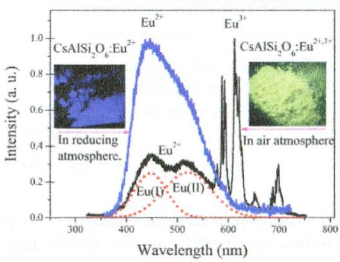

835 dx.doi.org/10.1021/ic402921b

Uranyl(VI) Complexes in and from Imidazolium Acetate Ionic Liquids: Carbenes versus Acetates?

Oldamur Hollóczki*

Dissolved in 1-alkyl-3-methylimidazolium acetate-based ionic liquids, uranyl(VI) cations are likely to form carbene complexes via a reaction with the solvent itself. This theoretically predicted reaction here can be generalized into a simple and convenient synthetic approach to produce carbene complexes from a wide variety of metal salts, allowing a further advance in the fields of NHC-metal complexes and catalysis.

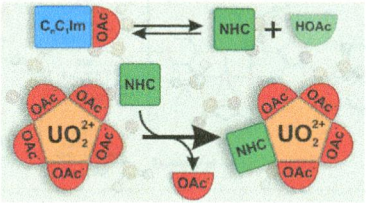

847 dx.doi.org/10.1021/ic402182j

Design and Syntheses of Electron-Transfer Photochromic Metal–Organic Complexes Using Nonphotochromic Ligands: A Model Compound and the Roles of Its Ligands

Cui-Juan Zhang, Zi-Wei Chen, Rong-Guang Lin, Ming-Jian Zhang, Pei-Xin Li, Ming-Sheng Wang,* and Guo-Cong Guo*

Constructing electron-transfer photochromic materials using nonphotochromic electron-donating/-accepting ligands may offer great opportunities to find new photochromic materials. The model compound $[Zn(HCOO)_2(4,4'\text{-bipy})]$ (**1**) was chosen to demonstrate the effectiveness of this design strategy. Its electron-transfer photochromic behavior has been discovered for the first time, and the roles of ligands have also been revealed on the basis of experimental and theoretical data. A high-contrast photoluminescence switch of **1** and the similarity of photochromic behavior between **1** and viologen compounds have also been found.

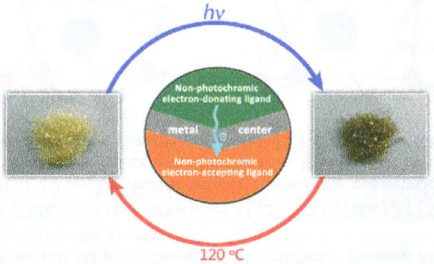

852 dx.doi.org/10.1021/ic402193x

Efficient Fluorinating Agent through Topochemical Fluorination of Co–Fe Layered Double Hydroxides

Nicolas Louvain,* Jérémy Peyroux, Marc Dubois, Wikenson Simond, and Fabrice Leroux

Mixed-metal inorganic fluoride, $Co_{0.60}Fe_{0.40}F_3$, solid solutions are obtained through topochemical reactions of $Co_2FeCl(OH)_6 \cdot 2H_2O$ LDH with molecular fluorine, F_2, at temperatures as low as 100 °C. This solid solution possesses interesting $F^\bullet$-releasing ability, and its efficiency as a solid-state fluorinating agent is demonstrated on a commercial polyethylene film. ^{19}F solid state NMR and contact angle measurements underline the efficient fluorination of this polymer.

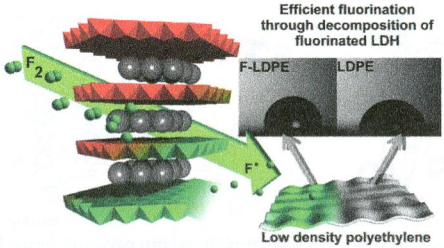

861 dx.doi.org/10.1021/ic402930d

Labile Degree of Disorder in Bismuth-Oxophosphate Compounds: Illustration through Three New Structural Types

A. Aliev, D. Endara, M. Huvé, M. Colmont, P. Roussel, L. Delevoye, T.T. Tran, P.S. Halasyamani, and O. Mentré*

Bismuth oxysalts are mainly built on oxocentered $O(Bi,M)_4$ tetrahedral units. This architectural principle favors a great degree of disorder, especially in the copresence of interstitial PO_4 groups delimiting 1D channels with strong chemical and structural flexibility. Here, we show, through three new compounds, gradual structural behaviors from completely disordered to fully ordered, eventually through organization in complex superlattices. Short-, medium-, and long-range ordering appear to be in competition in these systems.

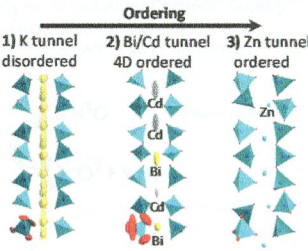

872 dx.doi.org/10.1021/ic402106v

From Hydrated $Ni_3(OH)_2(C_8H_4O_4)_2(H_2O)_4$ to Anhydrous $Ni_2(OH)_2(C_8H_4O_4)$: Impact of Structural Transformations on Magnetic Properties

Adel Mesbah,* Pierre Rabu, Romain Sibille, Sébastien Lebègue, Thomas Mazet, Bernard Malaman, and Michel François

Dehydration of the hybrid compound $[Ni_3(OH)_2(tp)_2(H_2O)_4]$ (**1**) upon heating led to the sequential removal of coordinated water molecules to give $[Ni_3(OH)_2(tp)_2(H_2O)_2]$ (**2**) at $T_1 = 433$ K and thereafter anhydrous $[Ni_2(OH)_2(tp)]$ (**3**) at $T_2 = 483$ K. **1** was found to be antiferromagnetic at $T_N = 4.11$ K, with metamagnetic behavior with a threshold field H_c of ca. 0.6 T. Compound **2** exhibits canted antiferromagnetism below $T_N = 3.19$ K, and **3** is ferromagnetic below $T_C = 4.5$ K.

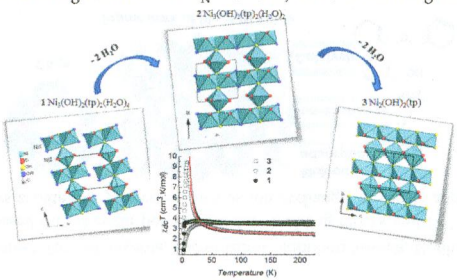

882 dx.doi.org/10.1021/ic402198a

Molecular Promoting of Aluminum Metal–Organic Framework Topology MIL-101 by *N,N*-Dimethylformamide

Maarten G. Goesten,* Pieter C. M. M. Magusin, Evgeny A. Pidko,* Brahim Mezari, Emiel J. M. Hensen, Freek Kapteijn, and Jorge Gascon*

In situ NMR and DFT modeling demonstrate that *N,N*-dimethylformamide (DMF) promotes the formation of metal–organic framework NH_2–MIL-101(Al). In situ NMR studies show that DMF forms a H–Cl–DMF complex during synthesis. This reaction induces a transformation from the MOF-235 topology into the MIL-101 topology. Electronic structure density functional theory (DFT) calculations show that the use of DMF instead of water as the synthesis solvent decreases the energy gap between the kinetically favored MIL-101 and thermodynamically favored MIL-53 products.

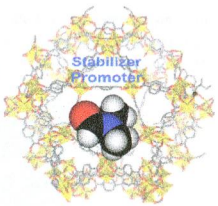

888 dx.doi.org/10.1021/ic402237b

Synthesis and Characterization of Calcium *N,N*-Dimethylaminodiboranates as Possible Chemical Vapor Deposition Precursors

Andrew C. Dunbar and Gregory S. Girolami*

The synthesis of the calcium *N,N*-dimethylaminodiboranate compound $Ca(H_3BNMe_2BH_3)_2$, **1**, and its adducts with diethyl ether, thf, dme, diglyme, tmeda, and 12-crown-4 are described; the crystal structures of the adducts are reported. The dme adduct is volatile and may serve as a precursor for the chemical vapor deposition of thin films containing calcium.

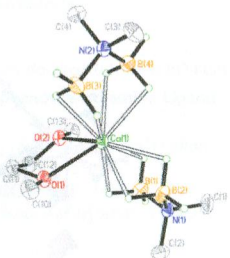

897 dx.doi.org/10.1021/ic4022596

Solvothermal Synthesis of Four Polyoxometalate-Based Coordination Polymers Including Diverse Ag(I)···π Interactions

Min-Xia Liang, Chan-Zi Ruan, Di Sun, Xiang-Jian Kong,* Yan-Ping Ren,* La-Sheng Long, Rong-Bin Huang, and Lan-Sun Zheng

Four polyoxometalate-based coordination polymers including diverse Ag(I)···π interactions have been obtained by solvothermal reaction of $AgNO_3$ and 5-phenyl-1*H*-tetrazole (Hptz) ligand in the presence of four types of polyoxometalates.

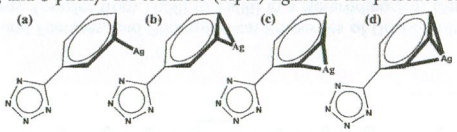

903 dx.doi.org/10.1021/ic4022849

Tetrahedral Connection of ε-Keggin-type Polyoxometalates To Form an All-Inorganic Octahedral Molecular Sieve with an Intrinsic 3D Pore System

Zhenxin Zhang, Masahiro Sadakane,* Toru Murayama, Shoko Izumi, Nobuhiro Yasuda, Norihito Sakaguchi, and Wataru Ueda*

A crystalline Mo−V−Bi oxide based on ε-Keggin polyoxometalate building blocks and Bi^{3+} linker has open micropores in diamondoid topology, and shows zeolite-like properties such as ion-exchange, molecule adsorption, and acid catalysis.

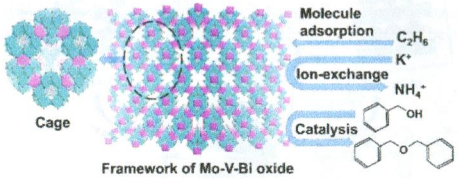

912 S dx.doi.org/10.1021/ic4022905

Component Analysis of Dyads Designed for Light-Driven Water Oxidation

Lars Kohler, Nattawut Kaveevivitchai, Ruifa Zong, and Randolph P. Thummel*

Seven photosensitizer-catalyst dyads are synthesized using three bridging ligands based on either a pyrimidine or pyrazine linker. The efficiency of light-driven water oxidation by these dyads depends on the magnitude of the sensitizer excited state reduction potential.

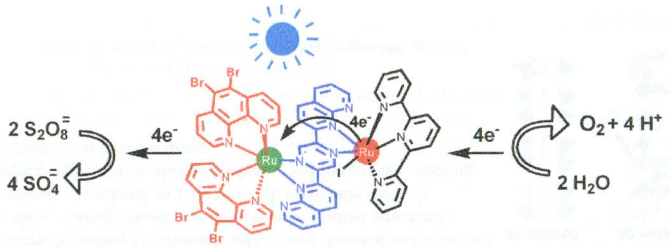

922 S dx.doi.org/10.1021/ic4023135

Luminescent Dirhenium(I)-Double-Heterostranded Helicate and Mesocate

Bhaskaran Shankar, Saugata Sahu, Naina Deibel, David Schweinfurth, Biprajit Sarkar, Palani Elumalai, Deepak Gupta, Firasat Hussain, Govindarajan Krishnamoorthy, and Malaichamy Sathiyendiran*

Self-assembly of luminescent, heteroleptic, neutral dirhenium-based unsaturated double-hetero-stranded helicate (**1**) and mesocate (**2**) was achieved from partially protected tritopic metal acceptor *fac*-$Re(CO)_3$, a flexible bis(monodentate) N donor, and flexible bis(bidentate) NᐱO donors.

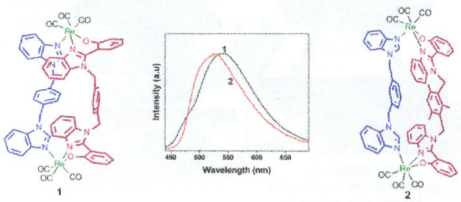

931 dx.doi.org/10.1021/ic402326b

Reinvestigation of the Total Li^+/H^+ Ion Exchange on the Garnet-Type $Li_5La_3Nb_2O_{12}$

Franck Gam, Cyrille Galven, Alain Bulou,* Françoise Le Berre,* and Marie-Pierre Crosnier-Lopez

Li^+/H^+ exchange was performed on the garnet $Li_5La_3Nb_2O_{12}$. The thermogravimetric analysis coupled with mass spectrometry, flame photometry, and Raman experiments showed unambiguously that the Li^+/H^+ exchange was not total and that some CH_3COOH remained bound to the garnet grain. In order to obtain the true exchange rate from TGA analysis, a washing step in ethanol is essential to remove the acid.

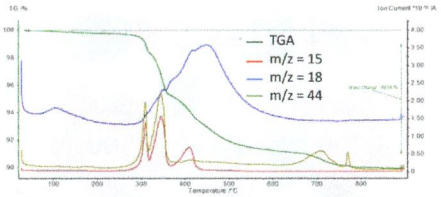

935 dx.doi.org/10.1021/ic402338q

Self-Assembly Synthesis, Structural Features, and Photophysical Properties of Dilanthanide Complexes Derived from a Novel Amide Type Ligand: Energy Transfer from Tb(III) to Eu(III) in a Heterodinuclear Derivative

Cunji Gao, Alexander M. Kirillov, Wei Dou, Xiaoliang Tang, Liangliang Liu, Xuhuan Yan, Yujie Xie, Peixian Zang, Weisheng Liu, and Yu Tang*

The first example of a [2 + 2] rectangular macrocycle heterodinuclear EuTb complex has been self-assembled from a novel amide type ligand. The Tb(III)-to-Eu(III) energy transfer in this dilanthanide compound has been investigated in detail.

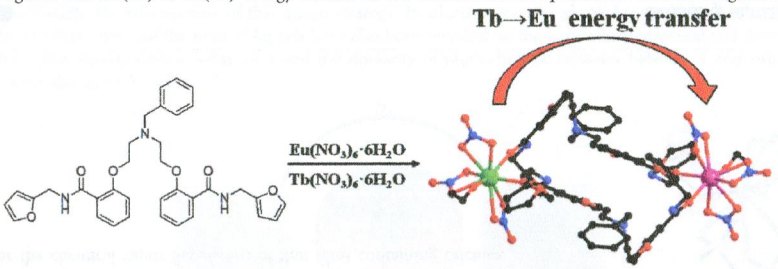

943 dx.doi.org/10.1021/ic4023486

Lanthanum Molybdate Nanoparticles from the Bradley Reaction: Factors Influencing Their Composition, Structure, and Functional Characteristics as Potential Matrixes for Luminescent Phosphors

Sarah Abtmeyer, Robert Pązik, Rafał J. Wiglusz, Małgorzata Małecka, Gulaim A. Seisenbaeva, and Vadim G. Kessler*

Precursor transformation as a function of the temperature of the thermal treatment allowed the structural changes of the intermediates and formation of $La_2Mo_2O_9$:Sm^{3+} to be followed. Heating to $\geq$700 °C leads to a mixture of α- and β-$La_2Mo_2O_9$ phases, introduction of smaller RE cations such as Sm^{3+} favors stabilization of the $La_{2-x}RE_xMo_2O_9$ phase with improved crystallinity even after lower-temperature thermal treatment, and the color of the produced luminescent phosphor can be tuned via controlling heat-treatment temperature.

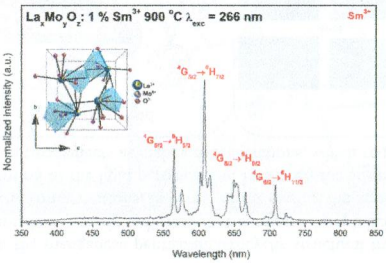

952 dx.doi.org/10.1021/ic4023745

Key Role of Bismuth in the Magnetoelastic Transitions of $Ba_3BiIr_2O_9$ and $Ba_3BiRu_2O_9$ As Revealed by Chemical Doping

Peter E. R. Blanchard, Zixin Huang, Brendan J. Kennedy, Samuel Liu, Wojciech Miiller, Emily Reynolds, Qingdi Zhou, Maxim Avdeev, Zhaoming Zhang, Jade B. Aitken, Bruce C. C. Cowie, Ling-Yun Jang, Thiam Teck Tan, Sean Li, and Chris D. Ling*

Magnetic susceptibility as a function of temperature for $Ba_3La_{1-x}Bi_xIr_2O_9$, showing suppression of the magnetic ordering with doping of the Bi site.

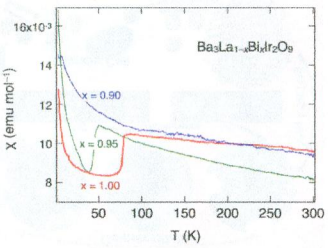

961 dx.doi.org/10.1021/ic4023954

Pulsed Electron Paramagnetic Resonance Spectroscopy of ^{33}S-Labeled Molybdenum Cofactor in Catalytically Active Bioengineered Sulfite Oxidase

Eric L. Klein, Abdel Ali Belaidi, Arnold M. Raitsimring, Amanda C. Davis, Tobias Krämer, Andrei V. Astashkin, Frank Neese, Günter Schwarz, and John H. Enemark*

A catalytically active SO variant with Moco labeled with ^{33}S ($I = 3/2$) has been produced by controlled *in vitro* synthesis with purified proteins. The ESEEM spectra at ~35 GHz are dominated by the "interdoublet" transition arising from the strong nuclear quadrupole interaction. The estimated experimental *hfi* and *nqi* parameters for ^{33}S (a_{iso} = 3 MHz and e^2Qq/h = 25 MHz) are in good agreement with those predicted by density functional theory.

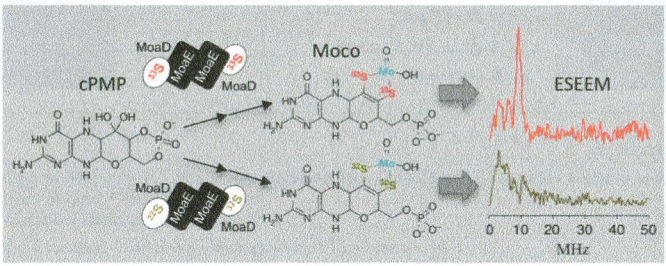

972 dx.doi.org/10.1021/ic4024458

Intramolecular C–H Oxidative Addition to Iridium(I) in Complexes Containing a *N,N'*-Diphosphanosilanediamine Ligand

Vincenzo Passarelli,* Jesús J. Pérez-Torrente, and Luis A. Oro

The intramolecular oxidative addition of the $SiCH_2$–H bond of $Si(CH_3)_2[(4\text{-}NC_6H_4CH_3)PPh_2]_2$ (SiNP) to iridium(I) affords the Ir(SiNP–H) platform featuring the κ^3C,P,P' coordination mode of the activated ligand $Si(CH_2)(CH_3)[(4\text{-}NC_6H_4CH_3)PPh_2]_2$ (SiNP–H). The iridium(III) and iridium(I) complexes of formula IrHCl(CO)(SiNP–H) and $Ir(SiNP–H)(CO)_2$ have been fully characterized in solution, and, in addition, the solid-state structure of $Ir(SiNP–H)(CO)_2$ has also been determined.

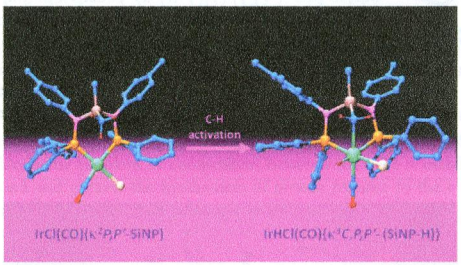

981 dx.doi.org/10.1021/ic402448p

Nitrosyl-Centered Redox and Acid–Base Interconversions in $[Ru(Me_3[9]aneN_3)(bpy)(NO)]^{3,2,1+}$. The pK_a of HNO for its Nitroxyl Derivative in Aqueous Solution

Nicolás Osa Codesido, Thomas Weyhermüller, José A. Olabe, and Leonardo D. Slep*

Characterization of $\{RuNO\}^{6,7,8}$ species in aqueous solution provides insight into the acid–base properties of bound HNO

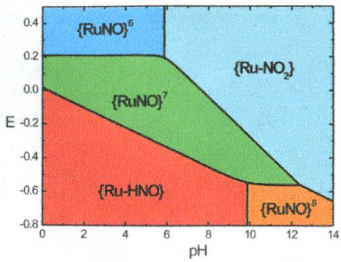

998 dx.doi.org/10.1021/ic402468k

Surfactant-Free Synthesis, Luminescent Properties, and Drug-Release Properties of LaF_3 and $LaCO_3F$ Hollow Microspheres

Ruichan Lv, Shili Gai,* Yunlu Dai, Fei He, Na Niu, and Piaoping Yang*

Uniform LaF_3 and $LaCO_3F$ hollow microspheres were synthesized through a two-step surfactant-free route under mild conditions. The phase and structure can easily be tuned by adjusting the pH value. The sample exhibited doxorubicin sustained and release properties, especially allowing it to be tracked or monitored by the luminescence of the functional carrier.

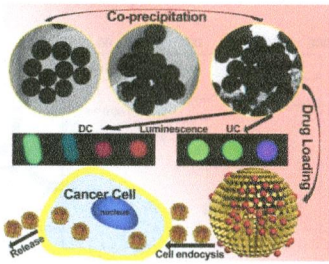

1009 dx.doi.org/10.1021/ic402469t

Amphiphilic Pentaazamacrocyclic Manganese Superoxide Dismutase Mimetics

Dominik Lieb, Isabell Kenkell, Jan Lj. Miljković, Daniel Moldenhauer, Nadine Weber, Milos R. Filipović, Franziska Gröhn, and Ivana Ivanović-Burmazović*

Amphiphilic SOD mimetics based on the manganese pentaazamacrocyclic structural framework have been synthesized and characterized. The tests on cell cultures have clearly indicated that increased lipophilicity enhances the beneficial biological effects of this type of complexes at low concentrations, in terms of decreasing the superoxide level in the cytosol and mitochondria, as well as on the prevention of the lipid peroxidation. However, the advantageous effects come also with price, i.e., the increased lipophilicity results in toxic effects at higher concentrations, which requires further structural optimizations.

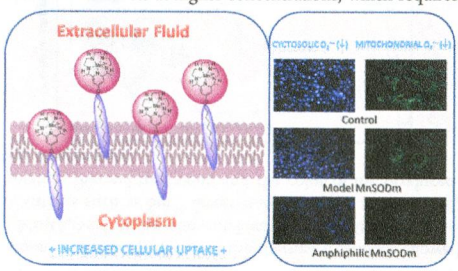

1021 S dx.doi.org/10.1021/ic4024713

Electrochemistry, Chemical Reactivity, and Time-Resolved Infrared Spectroscopy of Donor–Acceptor Systems [(Q^x)Pt(pap^y)] (Q = Substituted *o*-Quinone or *o*-Iminoquinone; pap = Phenylazopyridine)

Naina Deibel, David Schweinfurth, Stephan Hohloch, Milan Delor, Igor V. Sazanovich, Michael Towrie, Julia A. Weinstein,* and Biprajit Sarkar*

Donor–acceptor complexes of platinum(II) with noninnocent ligands are reported. The electronic structures, redox-induced reactivity, and excited-state dynamics in these complexes have been investigated by a combination of electrochemical, spectroscopic, and theoretical methods.

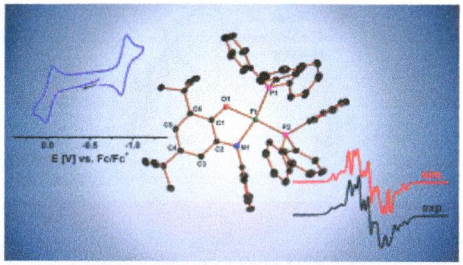

1032 S dx.doi.org/10.1021/ic402481b

Construction of Two Microporous Metal–Organic Frameworks with flu and pyr Topologies Based on $Zn_4(\mu_3\text{-}OH)_2(CO_2)_6$ and $Zn_6(\mu_6\text{-}O)(CO_2)_6$ Secondary Building Units

Xing-Jun Li, Fei-Long Jiang, Ming-Yan Wu, Lian Chen, Jin-Jie Qian, Kang Zhou, Da-Qiang Yuan, and Mao-Chun Hong*

A tripodal phosphoric carboxylate ligand, tris(4-carboxylphenyl)phosphineoxide (H_3TPO), has been used to construct two novel microporous metal–organic frameworks, which contain rare butterfly-shaped $Zn_4(\mu_3\text{-}OH)_2(CO_2)_6$ and octahedral $Zn_6(\mu_6\text{-}O)(CO_2)_6$ secondary building units and show 4,8-connected flu and 3,6-connected pyr topologies, respectively. Large cavities and one-dimensional channels are observed in these two frameworks. Gas-sorption measurements indicate that complex **2** has a good H_2 uptake capacity of 171.9 $cm^3\ g^{-1}$ (1.53 wt %) at 77 K and 1.08 bar, and its ideal adsorbed solution theory calculation predicts highly selective adsorption of CO_2 over N_2 and CH_4.

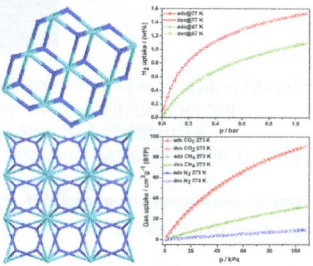

1039 Ⓢ dx.doi.org/10.1021/ic4025102

Ligand Dynamics of *tert*-Butyl Isocyanide Oxido Complexes of Molybdenum(IV)

Jana Leppin, Christoph Förster, and Katja Heinze*

The six-coordinate molybdenum(IV) oxido isocyanide complex **1** equilibrates with the diastereomer **2** in solution at ambient temperature via a trigonal-twist mechanism with dissociation of the imine nitrogen donor of one chelate ligand (hemilabile ligand) rather than with dissociation of the monodentate isocyanide ligand. The isomerization barrier has been experimentally determined as 91 and 95 kJ mol^{-1} in tetrahydrofuran and toluene, respectively.

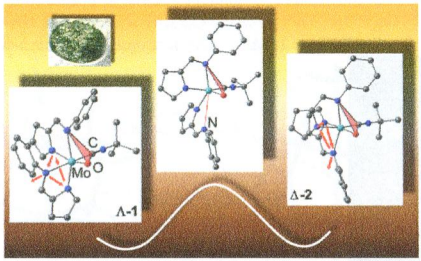

1048 dx.doi.org/10.1021/ic402525w

Influence of Ce Substitution for Bi in $BiVO_4$ and the Impact on the Phase Evolution and Microwave Dielectric Properties

Di Zhou,* Li-Xia Pang, Jing Guo, Ze-Ming Qi, Tao Shao, Qiu-Ping Wang, Hui-Dong Xie, Xi Yao, and Clive A. Randall

The $(Bi_{0.75}Ce_{0.25})VO_4$ ceramic, which was densified below 900 °C and consisted of both zircon and scheelite phases, was found to possess a permittivity of ~47.9, a Q_f value of ~18000 GHz, and a near-zero temperature coefficient of ~+15 ppm/°C at 7.6 GHz and is stable in a wide temperature range between 20 and 140 °C. Grains belonging to the zircon and scheelite phases could be clearly distinguished from each other from the EBSD phase map.

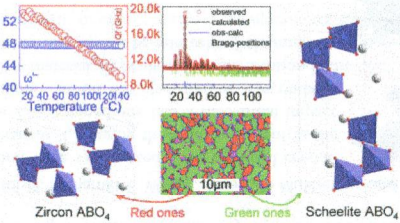

1056 Ⓢ dx.doi.org/10.1021/ic4025348

Structural Disorder in $AMoO_4$ (A = Ca, Sr, Ba) Scheelite Nanocrystals

Federico A. Rabuffetti, Sean P. Culver, Leopoldo Suescun, and Richard L. Brutchey*

The crystal structure of sub-15 nm $AMoO_4$ (A = Ca, Sr, Ba) scheelite nanocrystals was investigated using a dual-space approach that combines Rietveld and pair distribution function analysis of X-ray diffraction data. Comparison of the average and local crystal structures indicates the presence of static orientational disorder of the MoO_4 tetrahedra. Results highlight the significance of coupling Rietveld and pair distribution function analysis to achieve an accurate description of the atomic arrangement in nanocrystals.

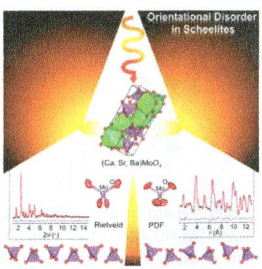

1062 dx.doi.org/10.1021/ic4025603

Combined Time-Resolved Laser Fluorescence Spectroscopy and Extended X-ray Absorption Fine Structure Spectroscopy Study on the Complexation of Trivalent Actinides with Chloride at T = 25–200 °C

Andrej Skerencak-Frech,* Daniel R. Fröhlich, Jörg Rothe, Kathy Dardenne, and Petra J. Panak

The complexation of trivalent curium and americium with chloride is studied by means of time-resolved laser fluorescence spectroscopy (Cm(III)) and extended X-ray absorption fine structure spectroscopy (Am(III)) in the temperature range of 25–200°C. The experiments are performed in a custom-built high-temperature cell which is modified for the respective spectroscopic technique.

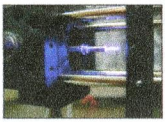

$$Cm^{3+} + n\,Cl^- \rightleftharpoons CmCl_n^{3-n}$$

$$TRLFS + SIT, EXAFS \quad T = 25 - 200°C \Rightarrow \log K_n^0(T), \varepsilon_{i,k}(T), \Delta_r H_m^0, \Delta_r S_m^0, \Delta_r C_{p,m}^0, Structure\ data$$

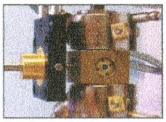

1070 (S) dx.doi.org/10.1021/ic402572h

Di-μ-oxo Dimetal Core of Mn^{IV} and Ti^{IV} as a Linker Between Two Chiral Salen Complexes Leading to the Stereoselective Formation of Different *M*- and *P*-Helical Structures

Takuya Kurahashi, Masahiko Hada, and Hiroshi Fujii*

We herein report the formation of di-μ-oxo dimanganese(IV) complexes with salen ligands, which selectively affords an *M*-helical dimer in the presence of the 3/3′-*tert*-butyl groups as a determinant steric factor. In contrast, the di-μ-oxo dititanium(IV) complex with the same salen ligand was previously reported to afford an opposite *P*-helical dimer. The present study clarifies that the difference arises from the covalency of M–O bonding, which generates a completely different framework for interligand interaction.

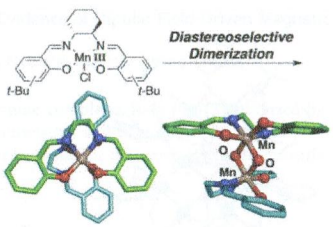

1080 (S) dx.doi.org/10.1021/ic4026206

Dihydrogen Bonding in Complex $(PP_3)RuH(\eta^1\text{-}BH_4)$ Featuring Two Proton-Accepting Hydride Sites: Experimental and Theoretical Studies

Natalia V. Belkova, Ekaterina V. Bakhmutova-Albert, Evgenii I. Gutsul, Vladimir I. Bakhmutov, Igor E. Golub, Oleg A. Filippov, Lina M. Epstein, Maurizio Peruzzini,* Andrea Rossin, Fabrizio Zanobini, and Elena S. Shubina*

Combined variable-temperature infrared and NMR spectroscopic and quantum-chemical (density functional theory and natural bond orbital) studies address the problem of competition between MH (M = metal) and BH hydrogens as proton-accepting sites in dihydrogen bond and unravel the mechanism of proton transfer to the complex $(PP_3)RuH(\eta^1\text{-}BH_4)$. The $B–H_{br}$ bond breaking is the common key step of all pathways investigated.

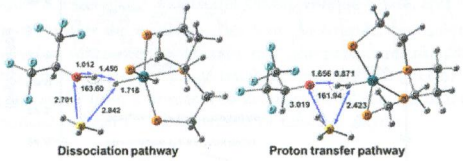

1091 S dx.doi.org/10.1021/ic402625s

Electronic Control of Discrimination between O_2 and CO in Myoglobin Lacking the Distal Histidine Residue

Ryu Nishimura, Tomokazu Shibata, Izumi Ishigami, Takashi Ogura, Hulin Tai, Satoshi Nagao, Takashi Matsuo, Shun Hirota, Osami Shoji, Yoshihito Watanabe, Kiyohiro Imai, Saburo Neya, Akihiro Suzuki, and Yasuhiko Yamamoto*

Using the stretching frequency of the Fe-bound carbon monoxide of myoglobin as a measure of the electron density of the heme Fe atom (ρ_{Fe}), the study revealed that the oxygen affinity of the H64L mutant decreases with a decrease in the ρ_{Fe} value and that the oxygen affinities of the mutant and native proteins are affected comparably by a given change in the ρ_{Fe} value.

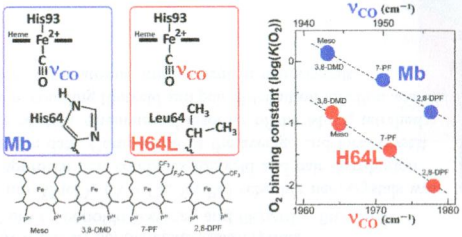

1100 S dx.doi.org/10.1021/ic402648f

Control of TiO_2 Grain Size and Positioning in Three-Dimensionally Ordered Macroporous TiO_2/C Composite Anodes for Lithium Ion Batteries

Nicholas D. Petkovich, Stephen G. Rudisill, Benjamin E. Wilson, Anwesha Mukherjee, and Andreas Stein*

Porous composites of TiO_2 and carbon were synthesized using colloidal crystal templates and a multiconstituent precursor. Changing the chelating agent in the precursor from trifluoroacetic acid to 2,4-pentanedione had a substantial impact on the TiO_2 crystal size and distribution. Carbon was also used as a secondary template to obtain a highly porous TiO_2 material. Crystallite size and location had a substantial impact on the ability of the composites to intercalate lithium.

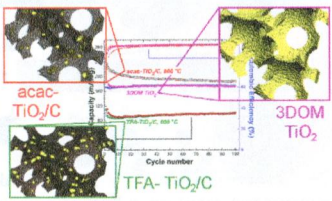

1113 S dx.doi.org/10.1021/ic402651k

Anionic Guests in Prismatic Cavities Generated by Enneanuclear Nickel Metallacycles

Jordi Esteban,* Mercè Font-Bardia, and Albert Escuer*

A Ni_9 metallamacrocycle generates a cryptand-like cavity that is able to coordinate azido and halide guests in a trigonal prismatic environment of hydrogen bonds.

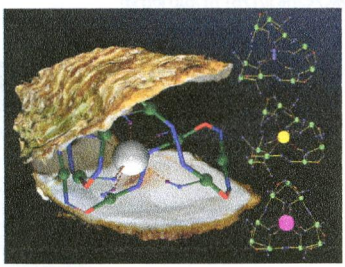

1122 S dx.doi.org/10.1021/ic4026798

Partial Spin Ordering and Complex Magnetic Structure in $BaYFeO_4$: A Neutron Diffraction and High Temperature Susceptibility Study

Corey M. Thompson,* John E. Greedan, V. Ovidiu Garlea, Roxana Flacau, Malinda Tan, Phuong-Hieu T. Nguyen, Friederike Wrobel, and Shahab Derakhshan

Powder neutron diffraction and magnetic susceptibility measurements have clarified the magnetic properties of $BaYFeO_4$. Below 48 K, the magnetic structure corresponds to a spin density wave, which transforms below 36 K to a cycloid structure. Both magnetic structures contain small ordered moments of Fe^{3+}, $\sim 3.0\mu_B$, indicating that a significant fraction of the moment remains paramagnetic down to 6 K. Susceptibility measurements indicates a broad maximum near 550 K indicative of short-range spin correlations.

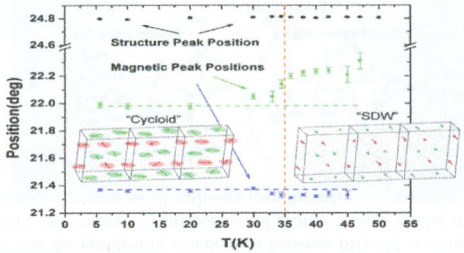

1128 S dx.doi.org/10.1021/ic4026816

Synthesis and Characterization of Nickel(II) Phosphonate Complexes Utilizing Pyridonates and Carboxylates as Co-ligands

Stuart K. Langley, Madeleine Helliwell, Simon J. Teat, and Richard E. P. Winpenny*

The use of carboxylates and pyridonates as co-ligands allow new nickel phosphonate cages to be structurally characterized. Magnetic studies show predominantly antiferromagnetic interactions between the spin centers.

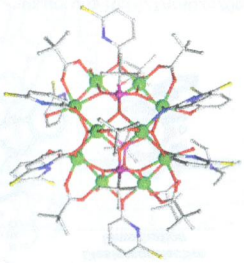

1135 dx.doi.org/10.1021/ic402687p

Electronic Structure of Ternary Rhodium Hydrides with Lithium and Magnesium

Jonas Nils Becker, Jessica Bauer, Andreas Giehr, Pui Ieng Chu, Nathalie Kunkel, Michael Springborg,* and Holger Kohlmann*

Using density-functional calculations, we study the rhodium−rhodium interactions in crystalline, ternary hydrides. Crystal Orbital Hamilton Populations are used to quantify the interactions. Structural properties and electronic densities of states are also reported.

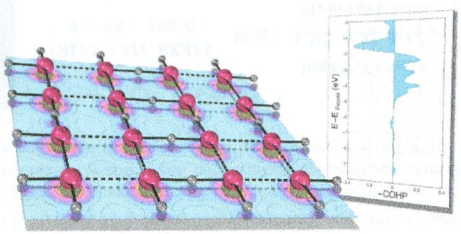

1144 S dx.doi.org/10.1021/ic4026987

Complexes Possessing Rare "Tertiary" Sulfonamide Nitrogen-to-Metal Bonds of Normal Length: *fac*-[Re(CO)$_3$(*N*(SO$_2$R)dien)]PF$_6$ Complexes with Hydrophilic Sulfonamide Ligands

Pramuditha L. Abhayawardhana, Patricia A. Marzilli, Frank R. Fronczek, and Luigi G. Marzilli*

Several new *fac*-[Re(CO)$_3$((RSO$_2$)N(CH$_2$CH$_2$NH$_2$)$_2$)]PF$_6$ complexes, despite having flexible chelate rings, possess very rare tertiary sulfonamide nitrogen-to-metal bonds of normal length. The R = Me complex exhibits an unusual upfield ^{13}C NMR signal consistent with sp^2-to-sp^3 rehybridization of the sulfonamide N upon coordination to Re^I. The R = tosyl complex is stable to heat in aqueous solution, indicating that *fac*-[M(CO)$_3$((RSO$_2$)N(CH$_2$CH$_2$NH$_2$)$_2$)]^n complexes are sufficiently robust to be utilized for radiopharmaceutical development (e.g., with M = $^{186/188}$Re).

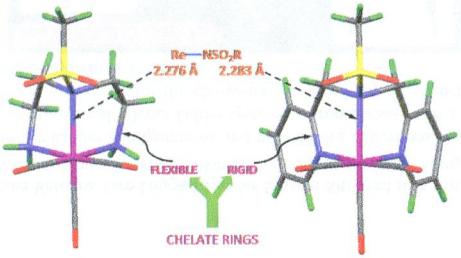

1156 S dx.doi.org/10.1021/ic4027199

Nature of Si−H Interactions in a Series of Ruthenium Silazane Complexes Using Multinuclear Solid-State NMR and Neutron Diffraction

Katharine A. Smart, Mary Grellier,* Yannick Coppel, Laure Vendier, Sax A. Mason, Silvia C. Capelli, Alberto Albinati, Virginia Montiel-Palma, Miguel A. Muñoz-Hernández, and Sylviane Sabo-Etienne*

The detailed analysis of Ru−Si−H interactions in new N-heterocyclic-silazane ruthenium complexes is reported. X-ray and neutron diffraction together with DFT studies enabled an accurate description of the molecular geometries and energies in complexes featuring RuSi$_3$H and RuSi$_3$H$_2^+$ systems.

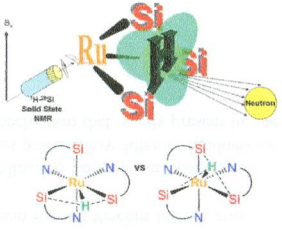

1166 S dx.doi.org/10.1021/ic402729g

Testing the Limits of the 18-Electron Rule: The Gas-Phase Carbonyls of Sc$^+$ and Y$^+$

Antonio D. Brathwaite, Jonathon A. Maner, and Michael A. Duncan*

Scandium and yttrium carbonyl cations produced in the gas phase via laser vaporization are mass selected and studied with infrared laser spectroscopy in the C−O stretching region. Mass spectra, ion fragmentation behavior, and infrared spectra, complemented by computational chemistry, establish the coordination numbers and structures of these complexes. Sc$^+$ does not form the eight-coordinate 18-electron complex but instead produces a 16-electron seven-coordinate species. However, Y$^+$ forms the anticipated eight-coordinate structure.

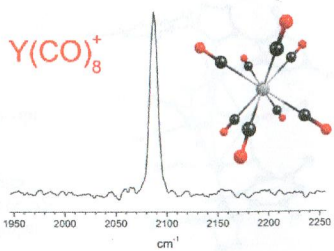

1170 dx.doi.org/10.1021/ic402738b

Role of the Acceptor in Tuning the Properties of Metal [M(II) = Ni, Pd, Pt] Dithiolato/Dithione (Donor/Acceptor) Second-Order Nonlinear Chromophores: Combined Experimental and Theoretical Studies

Davide Espa, Luca Pilia, Christodoulos Makedonas, Luciano Marchiò, M. Laura Mercuri, Angela Serpe, Alberto Barsella, Alain Fort, Christiana A. Mitsopoulou,* and Paola Deplano*

Structural properties of the title complexes strongly affect their electronic and NLO properties. Actually, the order of the dithione (donor ligand) torsion angle δ_2 correlates inversely with either the oscillator strength and $\mu\beta_0$.

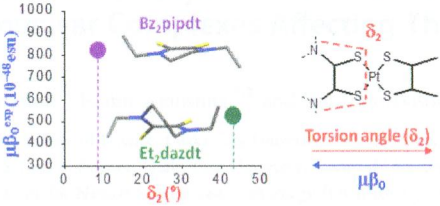

1184 dx.doi.org/10.1021/ic4027688

New Metal Phthalocyanines/Metal Simple Hydroxide Multilayers: Experimental Evidence of Dipolar Field-Driven Magnetic Behavior

Riadh Bourzami, Séraphin Eyele-Mezui, Emilie Delahaye, Marc Drillon, Pierre Rabu, Nathalie Parizel,* Sylvie Choua, Philippe Turek, and Guillaume Rogez*

A series of layered simple hydroxides functionalized by transition metal phthalocyanine complexes have been synthesized by anion exchange reaction and characterized by ancillary techniques. Magnetic measurements and X and Q-band EPR spectroscopy studies establish the strictly dipolar nature of the magnetic interaction between the inorganic layers and provide an estimation of the internal dipolar field (≈30 mT).

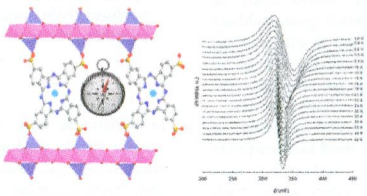

1195 dx.doi.org/10.1021/ic402795g

POP–Pincer Ruthenium Complexes: d^6 Counterparts of Osmium d^4 Species

Joaquín Alós, Tamara Bolaño, Miguel A. Esteruelas,* Montserrat Oliván, Enrique Oñate, and Marta Valencia

The Ru{xant(P^iPr_2)$_2$} metal fragment avoids the oxidation state four. As a result, the osmium d^4-polyhydrides are d^6-dihydrogen in the ruthenium chemistry, which require different synthetic procedures from those of osmium for their preparation. In addition, this Article shows that the hydride-tetrahydroborate RuH(η^2-H_2BH_2){xant(P^iPr_2)$_2$} is an efficient catalyst precursor for the hydrogen transfer from 2-propanol to ketones, the alkylations of nitriles and ketones with alcohols, and the regio- and stereoselective head-to-head (Z) dimerization of terminal alkynes.

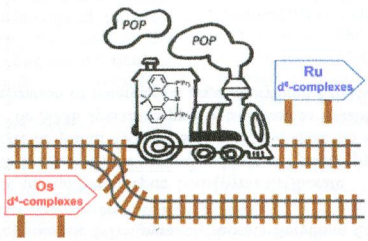

1210 S dx.doi.org/10.1021/ic402832b

Synthesis and Structural Characterization of Ruthenium Carbonyl Cluster Complexes Containing Platinum with a Bulky N-Heterocyclic Carbene Ligand

Sumit Saha and Burjor Captain*

The reaction of $Ru_3(CO)_{12}$ with $Pt(IMes)_2$ at room temperature afforded the monoplatinum–triruthenium cluster complex $Ru_3Pt(IMes)_2(CO)_{11}$, **1**, and the diplatinum–triruthenium cluster complex $Ru_3Pt_2(IMes)_2(CO)_{12}$, **2**. The reaction of $Ru(CO)_5$ with $Pt(IMes)_2$ in at 0 °C yielded the monoplatinum–diruthenium cluster complex $Ru_2Pt(IMes)(CO)_9$, **3**, and monoruthenium–diplatinum cluster complex $RuPt_2(IMes)_2(CO)_6$, **4**. The reaction of **2** with hydrogen at 80 °C afforded the tetrahydride–tetraruthenium complex $Ru_4(IMes)(CO)_{11}(\mu\text{-H})_4$, **5**, and dihydride–diruthenium–diplatinum complex $Ru_2Pt_2(IMes)_2(CO)_8(\mu\text{-H})_2$, **6**.

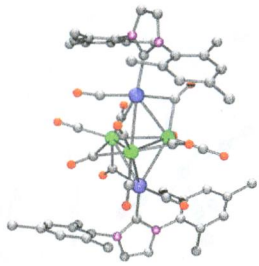

1217 S dx.doi.org/10.1021/ic402841d

Influence of Photoinduced Electron Transfer on Lanthanide-Based Coordination Polymer Luminescence: A Comparison between Two Pseudoisoreticular Molecular Networks

Stéphane Freslon, Yun Luo, Guillaume Calvez, Carole Daiguebonne,* Olivier Guillou,* Kevin Bernot, Vincent Michel, and Xiao Fan

The luminescent properties of two families of heteronuclear lanthanide-containing coordination polymers are compared. Despite similar chemical formulas, crystal structures, and hydration rates these two families present very different luminescent properties. These different optical behaviors can be attributed to the presence of a PET mechanism that is only present in one out of the two series.

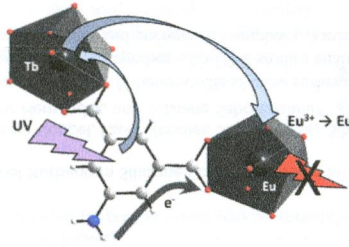

1229 S dx.doi.org/10.1021/ic402846v

Variable-Rung Design for a Mixed-Valence Two-Legged Ladder System Situated in a Dimensional Crossover Region

Kazuya Otsubo,* Atsushi Kobayashi, Kunihisa Sugimoto, Akihiko Fujiwara, and Hiroshi Kitagawa*

Rung variation offers a variety of intraladder configurations and periodic leg distortions associated with unique electronic properties of two-legged metal–organic mixed-valence ladder systems. In comparison with a single chain system, the obtained ladder materials show quite different tendencies for the charge-transfer band gap as a function of the distortion of the leg, indicating that an inherent electronic system is achieved.

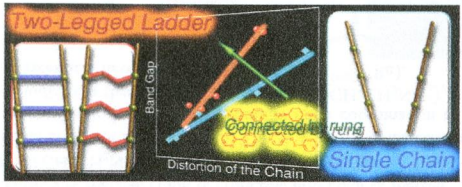

1241 Ⓢ dx.doi.org/10.1021/ic402895h

Synthesis and Characterization of Heteroleptic 1-Tris(pyrazolyl)borate Beryllium Complexes

Dominik Naglav, Dieter Bläser, Christoph Wölper, and Stephan Schulz*

The synthesis and crystal structures of several heteroleptic 1-tris(pyrazolyl)borate beryllium halides TpBeX (X = Cl **1**, Br **2**, I **3**, F **4**), the pyrazole adduct of TpBe(F)pyr (**5**) as well as the 1-tris(pyrazolyl)borate beryllium hydride, deuteride, and azide (H **6**, D **7**, N_3 **8**) is described. In addition, ^{9}Be-NMR spectroscopy is introduced as suitable analytical tool for the in situ characterization of heteroleptic organoberyllium halides, pseudohalides, and hydrides.

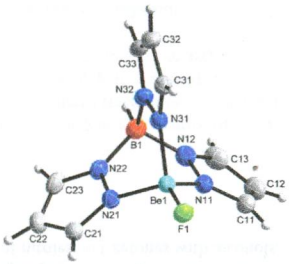

1250 Ⓢ dx.doi.org/10.1021/ic402929m

Noncentrosymmetric $YVSe_2O_8$ and Centrosymmetric $YVTe_2O_8$: Macroscopic Centricities Influenced by the Size of Lone Pair Cation Linkers

Yeong Hun Kim, Dong Woo Lee, and Kang Min Ok*

Two new vanadium selenite and tellurite, NCS $YVSe_2O_8$ and CS $YVTe_2O_8$, have been synthesized. The size of lone pair cation linkers plays a role in determining the macroscopic centricities of the materials.

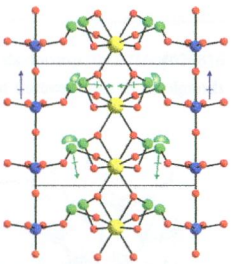

Ⓢ Supporting Information available via online article